AOARD Grant # FA23861114030

Ravi Pant and Benjamin J. Eggleton

CUDOS, University of Sydney 2006, AUSTRALIA

http://sydney.edu.au/science/physics/cudos/ egg@physics.usyd.edu.au

"Tunable stimulated Brillouin scattering in planar optical circuits"

Final Report

1. Statement of Problem:

Stimulated Brillouin Scattering (SBS), whereby light interacts coherently with acoustic phonons, is a powerful and flexible mechanism for the control of optical pulses, having recently been used to achieve tunable slow-light as well as find application in a range of important technologies such as Brillouin lasers, sensors, opto-mechanical oscillator and tailoring optical forces. Conversely, SBS is undesirable in many applications, one example of which is nonlinear optics, where it leads to output power saturation and must be suppressed. The ability to control (i.e. enhance or suppress) SBS in integrated optical chips is therefore key to the realization of many applications in modern photonics that involve light-sound and light-light interactions.

2. Program objective/Concept:

The objective of this program is to demonstrate tunable SBS viz. SBS enhancement and suppression and use it to demonstrate on-chip devices for slow-light based tunable delay, microwave photonics and nonlinear optics. The concept relies on tailoring the interaction between optical and acoustic modes using a combination of material, geometry and optical pump characteristics. While the choice of material and geometry enhances/suppresses SBS by controlling the overlap between the optical and acoustic modes; tuning the pump characteristics can be used to effectively suppress SBS and at the same time improving the efficiency of the nonlinear optical processes.

3. Approach

The approach to this project is to exploit the large SBS cross-section and small optical mode area of our chalcogenide (As_2S_3) rib waveguide to demonstrate on-chip SBS. Effect of SBS tuning (enhancement and suppression) is studied in a chalcogenide step-index fibre where it is used to demonstrate a novel way of writing multi-wavelength Hill gratings and a single Hill grating of increased strength.

4. Program progress to date

a) *Demonstration of on-chip SBS:* We demonstrated for the *first* time on-chip SBS in a single-pass geometry. Exciting SBS in a chip scale device requires generation of large Brillouin gain $G = g_B P_P L/A_{eff}$ in a short length, where g_B is the Brillouin gain coefficient, P_P is the pump power, L is the device length and A_{eff} is the effective optical mode area. Small Brillouin scattering cross-section and large A_{eff} of silica fiber, which is the commonly used platform for exploiting SBS, has prevented the generation of large G at chip scale without incurring large power consumption (~ 10's W).

Chalcogenide glass with its large nonlinear index of refraction (n_2), which results from its large refractive index (n), has been shown to be a competent platform for on-chip ultrafast all-optical signal processing. The large n of chalcogenide glass results in large Brillouin scattering cross-section due to its strong dependence on refractive

Report Documentation Page

Form Approved
OMB No. 0704-0188

1. REPORT DATE	2. REPORT TYPE	3. DATES COVERED
01 NOV 2012	**Final**	**01-02-2011 to 01-03-2012**

4. TITLE AND SUBTITLE
Tunable stimulated Brillouin scattering in photonic integrated circuits

5a. CONTRACT NUMBER
FA23861114030

5b. GRANT NUMBER

5c. PROGRAM ELEMENT NUMBER

6. AUTHOR(S)
Benjamin Eggleton

5d. PROJECT NUMBER

5e. TASK NUMBER

5f. WORK UNIT NUMBER

7. PERFORMING ORGANIZATION NAME(S) AND ADDRESS(ES)
University of Sydney,CUDOS, School of Physics A28,Sydney,NSW,AU,2006

8. PERFORMING ORGANIZATION REPORT NUMBER
N/A

9. SPONSORING/MONITORING AGENCY NAME(S) AND ADDRESS(ES)
AOARD, UNIT 45002, APO, AP, 96338-5002

10. SPONSOR/MONITOR'S ACRONYM(S)
AOARD

11. SPONSOR/MONITOR'S REPORT NUMBER(S)
AOARD-114030

12. DISTRIBUTION/AVAILABILITY STATEMENT
Approved for public release; distribution unlimited

13. SUPPLEMENTARY NOTES

14. ABSTRACT
Stimulated Brillouin Scattering (SBS), whereby light interacts coherently with acoustic phonons is a powerful and flexible mechanism for the control of optical pulses, having recently been used to achieve tunable slow-light as well as find application in a range of important technologies such as Brillouin lasers, sensors, opto-mechanical oscillator and tailoring optical forces. Conversely SBS is undesirable in many applications, one example of which is nonlinear optics, where it leads to output power saturation and must be suppressed. The ability to control (i.e. enhance or suppress) SBS in integrated optical chips is therefore key to the realization of many applications in modern photonics that involve light-sound and light-light interactions.

15. SUBJECT TERMS
photonic integrated circuits, brillouin scattering

16. SECURITY CLASSIFICATION OF:			17. LIMITATION OF ABSTRACT	18. NUMBER OF PAGES	19a. NAME OF RESPONSIBLE PERSON
a. REPORT	b. ABSTRACT	c. THIS PAGE			
unclassified	**unclassified**	**unclassified**	**Same as Report (SAR)**	**21**	

index ($\propto n^8$). However, having large n alone is not sufficient for strong light-sound interaction. Further restrictions are imposed by the requirement of strong optical-acoustic overlap, which requires both the optical and acoustic modes to be strongly confined in the same structure (see Fig. 1), and smaller optical mode area for efficient operation.

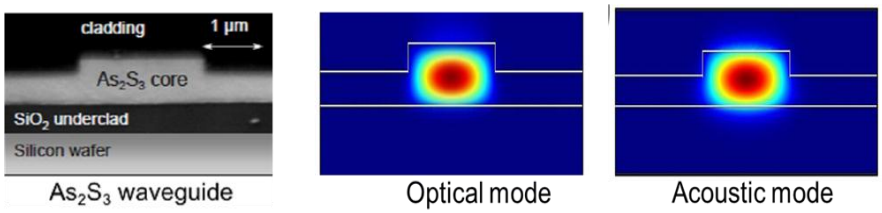

Fig. 1. Optical microscope image of a typical chalcogenide rib waveguide and calculated optical and acoustic modes

For a chalcogenide (As_2S_3) chip fabricated on a silica substrate, the large index contrast with the substrate enables fabrication of a device with small optical mode area (2.3 μm^2) and strong optical confinement. The smaller sound speed in chalcogenide glass (v_a ~ 2550 m/s) compared to silica (v_a ~ 5600 m/s) results in strong acoustic mode confinement (see Fig. 1) and thus strong light-sound interaction, making it the material of choice for chip-scale SBS.

SBS was characterized in a 7 cm long As_2S_3 rib waveguide using the backscattered spectrum and pump-probe measurements. Figure 2(a) shows the backscattered signal demonstrating the generation of Stokes signal as the average pump power is increased; pulsed pump with a duty cycle of 1% and pulse width of 400ns was used for backscattering experiment. From the backscattered measurements, a Brillouin frequency shift Ω_B ~ 7.7 GHz was obtained. Using the CW pump-probe technique, SBS gain spectrum was measured (see Fig. 2(b)) where the measured full-width at half-maximum (FWHM) linewidth was $\Delta\nu_B$ ~ 34 MHz, consistent with measured linewidth in chalcogenide fibres. From the measurements in Figs. 2(a) and (b), we calculate a Brillouin gain coefficient g_B ~ 0.74 x 10^{-9} m/W. The threshold peak pump power for the Stokes generation is P_{peak} ~ 2W.

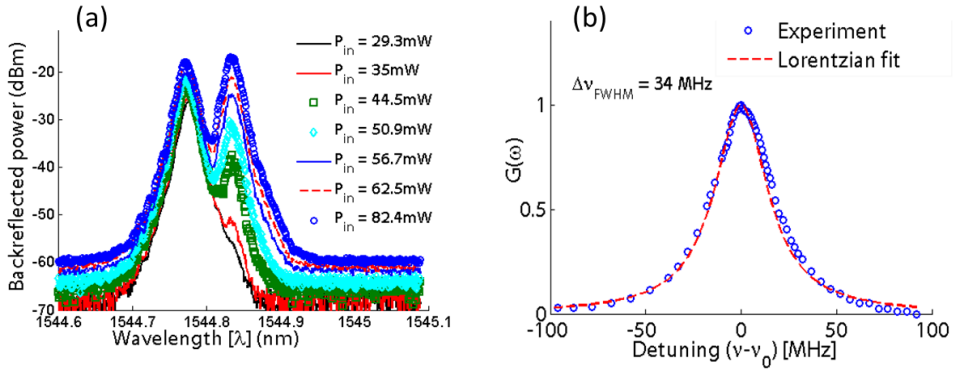

Fig. 2. Characterization of SBS in an As_2S_3 photonic chip using (a) backscattered spectrum demonstrating the generation and increase of the Stokes signal with increase in the pump power and (b) calculated and measured SBS gain profile. The gain profile was measured using the pump-probe technique.

b) *Cavity enhanced on-chip SBS*: In our SBS demonstration, the peak power required to excite on-chip SBS in a single-pass geometry is ~ 2W, which, although, is much smaller than the power required (~10's W) to excite SBS in the same length of silica fibre however; it is still significantly large for useful applications e.g. Brillouin lasers. Exploiting SBS in a chip-scale cavity enhances SBS and also results in cascaded effect whereby the Stokes signal acts as the pump to excite higher–order Stokes.

Cavity enhanced on-chip SBS was demonstrated in our photonic chip where the threshold peak power was reduced to ~ 0.5 W, which is four times smaller than the threshold for the single-pass geometry. The cavity was formed by using a chip without the anti-reflection coating. Fresnel reflection at the end facets gives rise to a reflectance ~ 17% which was enough to enhance the SBS process. Figures 3(a) and (b) show the SBS spectrum in the forward direction and the radio-frequency spectrum, respectively, demonstrating that the frequency of the second-order Stokes signal is twice the frequency of the Stokes signal. On-chip multi-Stokes SBS has the potential for chip-scale comb source and microwave source. Using a high reflectance cavity, threshold power can be reduced to ~ 10's mW, resulting in a compact, low-power comb and microwave source.

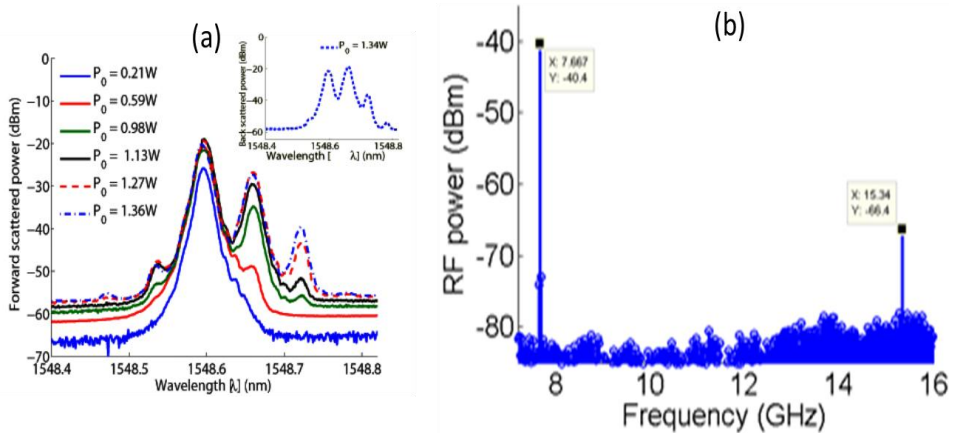

Fig. 3. Results for cavity enhanced on-chip SBS (a) forward scattered SBS spectrum showing multi-order Stokes and anti-Stokes signal, which arise from the four-wave mixing between the pump and co- propagating Stokes and (b) radio-frequency spectrum demonstrating that the beat signal between the pump and second-order Stokes occurs at twice the Brillouin shift. The inset of Fig. 3(a) shows the backscattered spectrum demonstrating the generation of up to 3 Stokes signal.

c) *On-chip SBS slow-light*: Stimulated Brillouin scattering (SBS) based slow and fast light has been at the forefront of techniques used for controlling light pulse speed due to its wavelength independence, room temperature operation, delay tunability and wide signal bandwidth range (MHz-GHz). While large tunable delays ($T_d = L\Delta n_g/c$) have been obtained using SBS slow- and fast-light in long length optical fibres (~ km), where Δn_g is the change in the group-index and c is the speed of light in vacuum, the actual slowing down factor has been very small in fiber based demonstrations due to small Δn_g. The best Δn_g achieved in an optical fiber is ~ 10, which was obtained in a 2 m long erbium doped bismuth fiber with a Brillouin gain ~ 53dB.

In our recent work, we exploit the large SBS cross-section and small-optical mode area of our chalcogenide photonic chip to realize SBS based slow and fast light. A large Δn_g ~ 130 was obtained in a 7cm long As_2S_3 rib waveguide with a gain of ~ 23 dB, which resulted in a delay of 23ns for a 100ns long Gaussian pulse and light

pulse speed of 2307 km/s. For a 25ns long Gaussian pulse, a delay of 22ns was measured, which corresponds to a fractional delay of nearly one pulse-width.

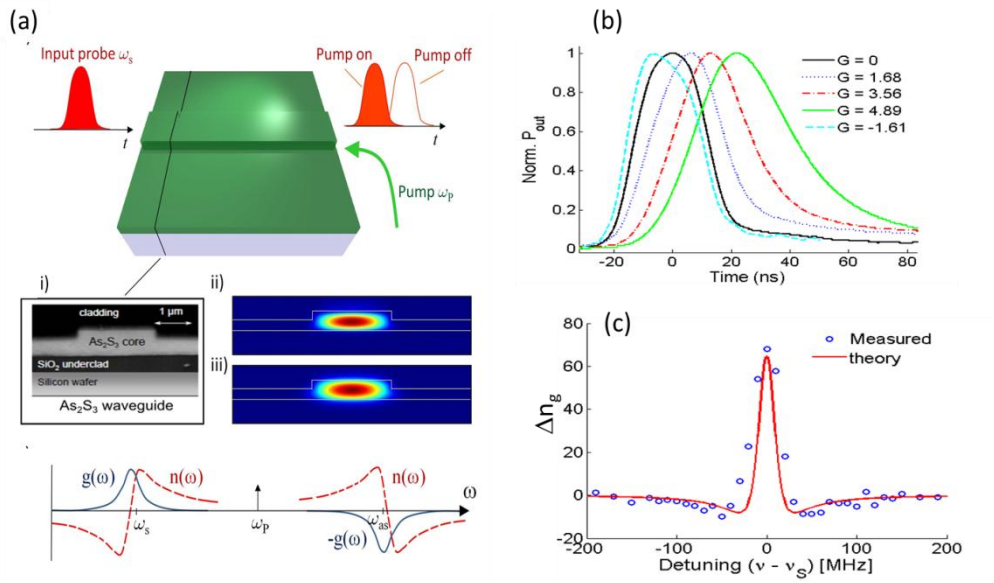

Fig. 4. (a) Schematic of on-chip SBS slow-light (b) pulse delay measurement for a 25 ns long Gaussian pulse demonstrating tunable delay of nearly one pulse width and fast light for the pulses centred at the anti-Stokes frequency and (c) group-index measurement for the slow-light regime demonstrating a large group-index of 68 at the Stokes frequency at a gain of ~ 11.3dB.

Figure 4(a) shows the schematic for on-chip SBS slow- and fast-light where a probe pulse interacts with a counter-propagating pump and experiences delay, which can be tuned by varying the pump power. For pulse delay measurements shown in Fig. 4(b), we used a quasi CW pump to increase the on-chip pump power. A maximum delay of 22 ns was measured for a 25 ns Gaussian pulse at a gain of ~ 23 dB. Fast light was observed for pulses centred at the anti-Stokes frequency (see Fig. 4(b)).

The group-index was measured for the *first* time for the SBS slow-light. In earlier fiber based SBS slow-light experiments, small change in n_g prevented the measurement of group-index. For the group-index measurement, delay of a low frequency sinusoidal signal was measured while the probe carrier frequency was detuned from the Stokes frequency. Group-index measurements were performed at gain of ~ 11.3 dB using a CW pump. Figure 4(c) shows the measured and calculated Δn_g for the slow light regime demonstrating a Δn_g ~ 68. For the fast light regime a negative group-index of -44 was measured. On-chip tunable delay using SBS slow-light opens up applications such as on-chip tap delay based microwave photonic filter (MPF) and true-time delay (TTD) for phased array antenna.

d) *Chip-based microwave photonic filter*: Narrowband, tunable and reconfigurable MPFs with high Q-factor are critical to microwave signal processing. Reconfigurable, narrowband MPFs with wide tuning range have been demonstrated using SBS in long length (~ 10-20km) optical fibres, which are incompatible with photonic integration. On-chip MPFs have been demonstrated using ring resonators; however demonstrated filter 3dB bandwidth (f_{3dB} ~ 1GHz) and small tuning range has resulted in very low Q-factor ~ 10.

Recently, we demonstrated a photonic chip based narrowband, reconfigurable, microwave photonic filter with large Q and wide tuning range. We exploit stimulated Brillouin scattering (SBS) in a 6.5 cm long chalcogenide (As_2S_3) photonic chip to demonstrate a MPF that exhibited a high quality factor Q ~ 520 and narrow bandwidth and was dynamically reconfigurable and widely tunable. It maintained a stable 3 dB bandwidth of 23 ± 2MHz (see Fig. 5(b)) and amplitude of 20 ± 2 dB (see Fig. 5(b)) over a large frequency tuning range of 2-12 GHz (See Fig. 5(a)).

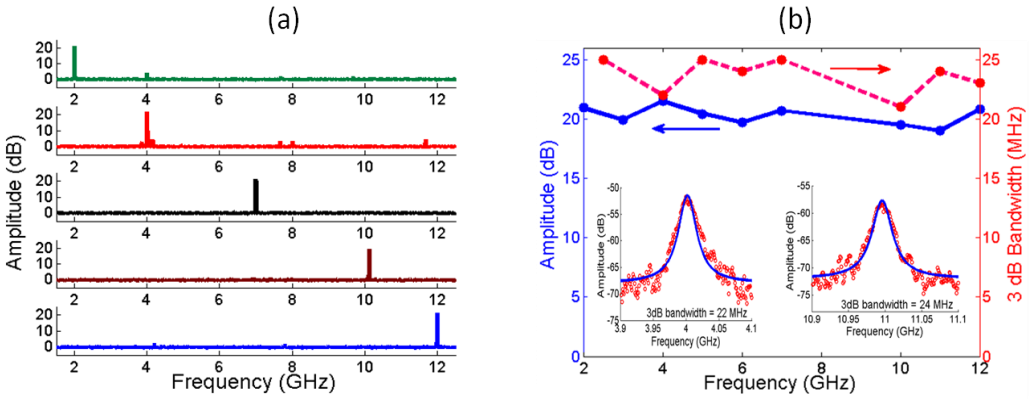

Fig.5. Photonic-chip based MPF response (a) demonstrating wide tuning range of 2-12 GHz for the MPF center frequency and (b) amplitude and f_{3dB} of PCMPF for different centre RF frequencies demonstrating good amplitude (~20 ± 2 dB) and bandwidth (23 ± 2 MHz) stability. Inset: MPF profiles taken at centre frequencies of 4 and 11 GHz.

By tailoring the pump spectrum, we reconfigured the 3 dB bandwidth of the MPF from ~20 MHz to ~40 MHz and tuned the shape factor S, defined as the ratio of 20dB bandwidth to 3dB bandwidth ($S=f_{20dB}/f_{3dB}$), from 3.5 to 2 resulting in a nearly flat-top filter profile (see Fig.6). This demonstration represents a significant advance in integrated microwave photonics with potential applications in on-chip microwave signal processing for RADAR and analog communications.

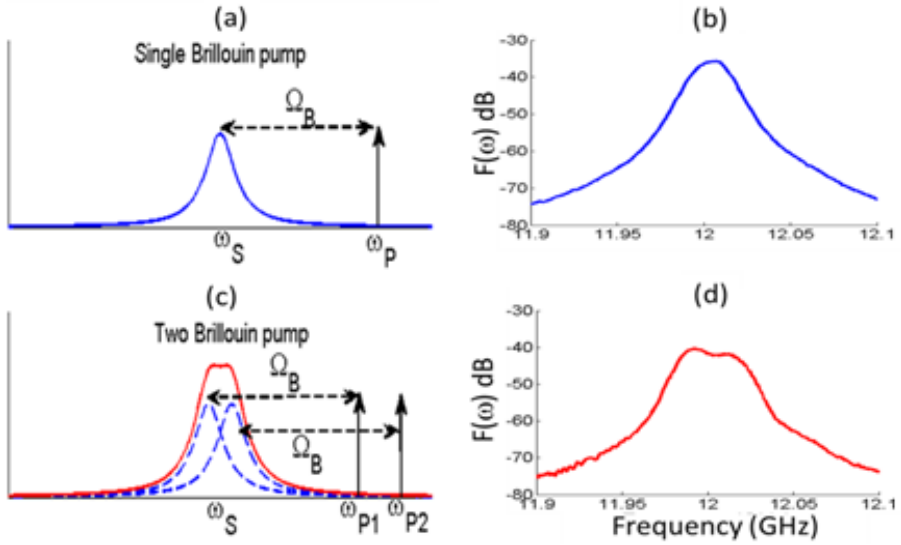

Fig. 6. Theoretical filter response for (a) single and (c) two pumps demonstrating MPF profile reshaping (flat top) with improved 3dB bandwidth. Measured MPF profiles for (b) single pump f_{3dB} ~ 20 MHz and (d) dual pump f_{3dB} ~ 40 MHz with shape factor improved from S=3.5 (single pump) to S=2 (dual pump). The reshaping results in flat topped filter profile.

e) *On-chip all-optical isolator*: One of the main challenges in all-optical integration is to realize a chip scale optical isolator. Faraday effect, which is used in most of the current optical isolators is a magnetic effect and results in a bulky device. In this study, we use the optical modes with parallel dispersion in our photonic chip to analyse a chip-based optical isolator. This concept was first introduced by Huang *et al.* in a 10m long optical fibre.

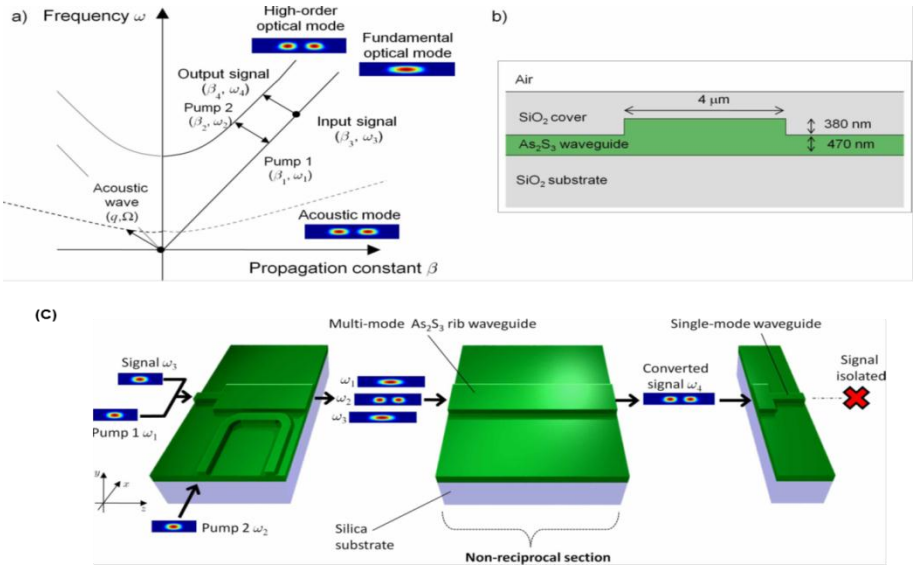

Fig. 7. (a) Principle of on-chip optical isolator exploiting forward SBS where two optical modes act as pumps to drive the acoustic field, which then acts as a mode converter for a signal launched in the fundamental modes at frequency ω_3, (b) schematic of the photonic chip used in isolator design and (c) proposed implementation of chip-based isolator.

Figure 7(a) shows the concept of on-chip all-optical isolation using forward SBS in a photonic chip shown in Fig. 7(b). Two optical modes with parallel dispersion curves are used as pumps to drive an acoustic mode at frequency $\Omega = \omega_1 - \omega_2$, where ω_1 and ω_2 are the frequencies of two optical modes. The signal to be isolated at frequency ω_3 is then co-propagated with the pumps and is converted to a higher-order optical mode at frequency ω_4. The mode at frequency ω_4 is then removed using a spatial filter resulting in optical isolation. The frequency range over which the dispersion curves are parallel determine the isolation bandwidth. Figure 7(c) shows the schematic of an on-chip optical isolator using forward SBS.

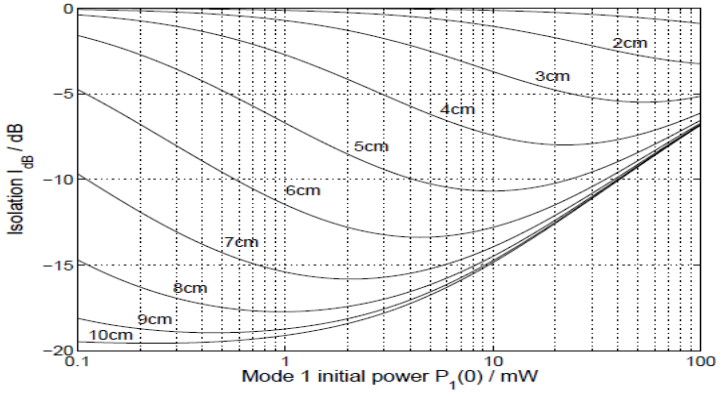

Fig. 8. Computed isolation for different device lengths as a function of initial power in pump 1 with power in pump 2 of $P_2(0)$ = 400 mW.

Figure 8 shows the computed isolation I_{dB} for waveguide lengths ranging from 2-10cm plotted as a function pump power in mode1. The power of pump 2 was kept fixed at $P_2(0)$ = 400 mW for these simulations, while the initial power in signal was $P_3(0)$ = 1μW. Maximum isolation of ~20dB was achieved in these simulations for a 10cm-long waveguide.

f) *Hill gratings using tunable SBS*: In this demonstration we exploit SBS enhancement to write Hill gratings with multiple wavelengths and SBS suppression to write a strong Hill gratings, demonstrating the usefulness of tunable SBS. Hill grating arises from beating of the counter-propagating signals of the same wavelength.

Figure 9a shows the effect of SBS suppression on Hill grating writing in a 3.6 cm long chalcogenide (As_2Se_3) fibre. Using a short pulse with pulse width T_{pulse} = 3.5ns SBS was suppressed, which resulted in a strong Hill grating with 7 dB reflection at the pump wavelength. Figure 9(a) shows the grating transmission (solid) and backscattered pump (dashed) with no Stokes generation. When long pulses (T_{pulse} = 25ns) were used in the experiment, SBS was enhanced and resulted in multi-order Stokes generation where each of the Stokes signal wrote its own grating albeit with smaller strength. Tuning SBS in a device can therefore be advantageous for writing multiple Hill gratings or a grating of increased strength.

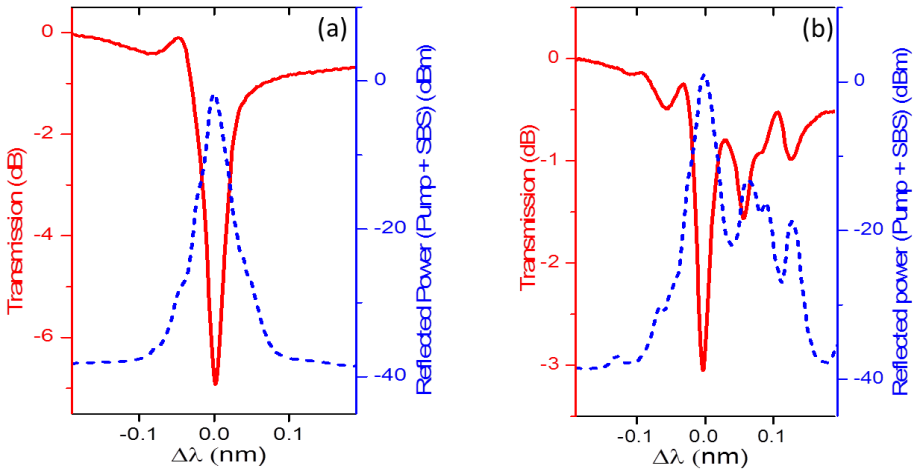

Fig. 9. Effect of SBS tuning by varying the pump pulse width on Hill grating writing in a 3.5 cm long step-index As_2Se_3 fibre (a) use of a short pulse (T_{pulse} = 3.5ns) results in SBS suppression and a stronger Hill grating (7dB reflection) and (b) using a long pulse (T_{pulse} = 25ns) results in SBS and its enhancement due to reflection at the fibre end facets leading to multi-Stokes generation and multi-wavelength Hill grating.

Journal publications

1. Ravi Pant, Christopher G. Poulton, Duk-Yong Choi, Hannah Mcfarlane, Samuel Hile, Enbang Li, Luc Thevenaz, Stephen J. Madden, Barry Luther-Davies, and Benjamin J. Eggleton,"On-chip stimulated Brillouin scattering," Optics Express 19, 8285-8290 (2011).

2. Ravi Pant, Enbang Li, Duk-Yong Choi, Christopher G. Poulton, Stephen J. Madden, Barry Luther-Davies, and Benjamin J. Eggleton,"Cavity enhanced stimulated Brillouin scattering in an optical chip for multiorder Stokes generation," Optics Letters 36, 3687-3689 (2011).

3. Ravi Pant, Adam Byrnes, Christopher G. Poulton, Enbang Li, Duk-Yong Choi, Stephen J. Madden, Barry Luther-Davies, and Benjamin J. Eggleton,"Photonic chip based tunable slow and fast light via stimulated Brillouin scattering," Optics Letters 37, 969-971 (2012).

4. Adam Byrnes, Ravi Pant, Enbang Li, Duk-Yong Choi, Christopher G. Poulton, Shanhui Fan, Steve Madden, Barry Luther-Davies, and Benjamin J. Eggleton, "Photonic chip based tunable and reconfigurable narrowband microwave photonic filter using stimulated Brillouin scattering," Optics Express 20, 18836-18845 (2012).

Invited talks and conference papers

5. Ravi Pant, Christopher Poulton, Hannah McFarlane, Luc Thevenaz, Duk-Yong Choi, Steve J. Madden, Barry Luther-Davies, and Benjamin J. Eggleton, "On-chip Stimulated Brillouin Scattering," CLEO, CTuX5, Baltimore, May 2011.

6. Ravi Pant, Christopher Poulton, Duk-Yong Choi, Enbang Li, Steve J. Madden, Barry Luther-Davies, and Benjamin J. Eggleton, "On-chip cascaded Stimulated Brillouin Scattering," IQEC/CLEO pacific rim, Sydney, August 2011.

7. Ravi Pant, and Benjamin J. Eggleton, "On-chip Stimulated Brillouin Scattering," **Invited talk**, SPIE Optics and Photonics, 8095-7, San Diego, August 2011.

8. Ravi Pant, Adam Byrnes, Christopher G. Poulton, Enbang Li, Duk-Yong Choi, Stephen J. Madden, Barry Luther-Davies, and Benjamin J. Eggleton, "Photonic chip based tunable slow and fast light via stimulated Brillouin scattering," CLEO, CF3M.2, San Jose, May 2012.

9. Adam Byrnes, Ravi Pant, Christopher G. Poulton, Enbang Li, Duk-Yong Choi, Stephen J. Madden, Barry Luther-Davies, and Benjamin J. Eggleton, "On-chip, tunable, narrow-bandpass microwave photonic filter using stimulated Brillouin scattering," CLEO, CTu2A.6, San Jose, May 2012.

10. Ravi Pant and Benjamin J. Eggleton, "On-Chip Slow and Fast Light Using Stimulated Brillouin Scattering," **Invited talk**, OSA Integrated Photonics Research (IPR), Colorado Springs, 17-21 June 2012.

11. Ravi Pant, Adam Byrnes, Enbang Li, Duk-Yong Choi, Christopher G. Poulton, Shanhui Fan, Steve Madden, Barry Luther-Davies, and Benjamin J. Eggleton,"Photonic chip based tunable and dynamically reconfigurable microwave photonic filter using stimulated Brillouin scattering," Nonlinear Photonics **Postdeadline**, Colorado Springs 17-21 June 2012.

12. Ravi Pant, and Benjamin J. Eggleton, "Slow light in optical circuits: harnessing on-chip stimulated Brillouin scattering," SPIE newsroom article, 2012.

13. Ravi Pant, and Benjamin J. Eggleton, "Slow light and microwave signal processing in optical circuits: harnessing on-chip stimulated Brillouin scattering," **Invited talk**, OSA Photonics India, IIT Chennai, India 9-12 Dec 2012.

Photonic-chip-based tunable slow and fast light via stimulated Brillouin scattering

Ravi Pant,[1,*] Adam Byrnes,[1] Christopher G. Poulton,[2] Enbang Li,[1] Duk-Yong Choi,[3] Steve Madden,[3] Barry Luther-Davies,[3] and Benjamin J. Eggleton[1]

[1]*Centre for Ultrahigh bandwidth Devices for Optical Systems (CUDOS), Institute of Photonics and Optical Science, School of Physics, The University of Sydney, New South Wales 2006, Australia*

[2]*CUDOS, University of Technology Sydney, Sydney, New South Wales 2007, Australia*

[3]*CUDOS, Laser Physics Centre, Australian National University, Canberra, Australian Capital Territory 0200, Australia*

**Corresponding author: rpant@physics.usyd.edu.au*

Received November 30, 2011; revised January 19, 2012; accepted January 20, 2012; posted January 23, 2012 (Doc. ID 159077); published March 1, 2012

We report the first (to our knowledge) demonstration of photonic chip based tunable slow and fast light via stimulated Brillouin scattering. Slow, fast, and negative group velocities were observed in a 7 cm long chalcogenide (As_2S_3) rib waveguide with a group index change ranging from ~ – 44 to +130, which results in a maximum delay of ~23 ns at a relatively low gain of ~23 dB. Demonstration of large tunable delays in a chip scale device opens up applications such as frequency sensing and true-time delay for a phased array antenna, where integration and delays ~10 ns are highly desirable. © 2012 Optical Society of America

OCIS Codes: 190.0190, 190.2640, 190.4360.

Control over the speed of light—*slow and fast light*—in a chip scale environment is fundamental to the development of devices for applications in quantum computing and information processing, optical communications and microwave signal processing, and sensing. Slow and fast light can be realized using the large dispersion associated with an induced or structural resonance [1]. Of all these techniques, the stimulated Brillouin scattering (SBS) based approach is the most flexible and practical for slow-light-based devices due to its wavelength independent nature, large signal bandwidth range (megahertz to gigahertz), room temperature operation, and delay tunability [2–12]. However, on-chip realization of SBS slow/fast light is difficult because the large group index change (Δn_g) required to achieve a significant delay ($\Delta T_d = L\Delta n_g/c$) in a small length ($L$), where c is speed of light in vacuum, is directly related to the Brillouin gain coefficient (g_B) and pump intensity (I_p), both of which have so far been constrained due to the material choice and device geometry.

Here we report the first demonstration of on-chip SBS slow and fast light using a 7 cm long rib waveguide based on chalcogenide glass (As_2S_3). While the large refractive index (n) of chalcogenide glass [11,13,14] leads to a large Brillouin gain coefficient ($g_B \sim 100 \times$ silica) due to its strong dependence on n ($g_B \propto n^8$)), strong optical and acoustic confinement [see Fig. 1(b)] in the rib structure provides large light–sound interaction and reduced optical mode area (A_{eff}) [14], which enhance the pump intensity at relatively low power.

SBS results from the interaction of light of frequency ω_P with an acoustic mode of frequency Ω_B. For a counterpropagating signal at frequency $\omega_s = \omega_p - \Omega_B$ (Stokes frequency), the three-wave interaction satisfies energy and momentum conservation and creates a gain resonance at ω_s [Fig. 1(c)]. For a signal centered at anti-Stokes frequency $\omega_{\text{as}} = \omega_p + \Omega_B$, an absorption resonance is created. Associated with these resonances is the large index change, which gives rise to slow and fast light.

Figure 1 shows the concept of on-chip SBS slow light where a pump of frequency ω_P is used to control the delay of a counterpagating Stokes wave [Fig. 1(a)]. The group delay experienced by a Stokes signal is then given by

$$\Delta T_d(\omega_s) = \frac{G}{\Gamma_B} = \frac{g_B I_p L_{\text{eff}}}{\Gamma_B}, \tag{1}$$

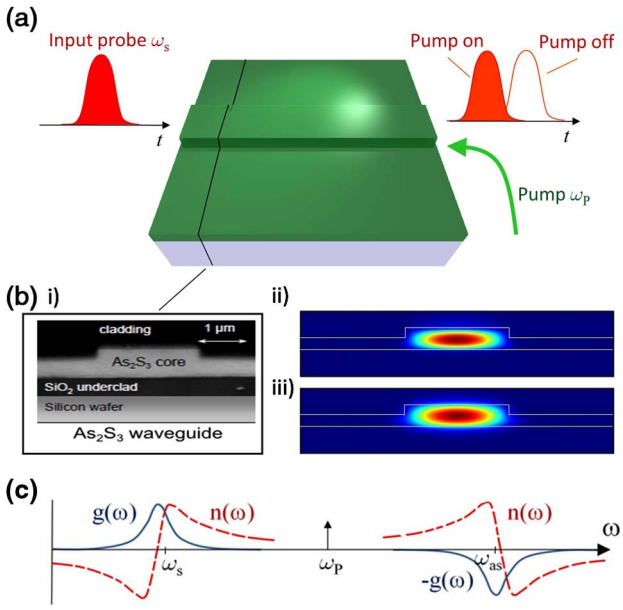

Fig. 1. (Color online) (a) Schematic of on-chip control of light pulse speed using SBS slow and fast light in a As_2S_3 rib waveguide; (b) (i) optical microscope image of a typical As_2S_3 rib waveguide and (ii) optical and (iii) acoustic modes in the rib waveguides showing strong mode confinement, which leads to strong light–sound interaction for SBS; (c) normalized gain and absorption resonances (solid blue curves) and associated dispersion (dashed red curves) demonstrating that the slope of dispersion is positive for slow light and negative for fast light.

where Γ_B is the Brillouin linewidth and $L_{\text{eff}} = (1 - e^{-\alpha L})/\alpha$ is the effective length, with L being the physical length and α being the propagation loss. From Eq. (1) it is evident that the delay can be tuned by varying the pump power (P_p). For an anti-Stokes signal, increase in P_p leads to increased absorption and thus fast light.

Figure 2 shows the experimental setup to realize on-chip SBS slow and fast light. The output delayed pulse was first filtered using an FBG setup to minimize the residual pump, which arises mainly from reflections at the lensed fiber and chip interface, and then amplified using a 200 mW, low-noise amplifier (EDFA2) before detection using a detector with 1 ns rise time. The optical chip used in the experiments had a cross-sectional area of 4 μm × 850 nm, $g_B \sim 0.74 \times 10^{-9}$ m/W [14], $A_{\text{eff}} \sim 2.3\ \mu\text{m}^2$, Brillouin shift of ~7.7 GHz, and linewidth of ~36 MHz. For the fast-light measurements the probe signal was amplified using a low-noise 200 mW EDFA to control the probe power, because the anti-Stokes wave is absorbed rather than amplified.

To measure the group index profile in the slow- (fast-) light regime, we modulated the probe signal centered at ω_s (ω_{as}) using a low-frequency sinusoidal wave. The probe carrier frequency was then detuned from $\omega_{s,\text{as}}$, while the coupled CW P_p was kept fixed. At each frequency detuning, the measured $\Delta T_d(\omega_{\text{probe}})$ was used to infer $\Delta n_g(\omega_{\text{probe}}) = c\Delta T_d(\omega_{\text{probe}})/L_{\text{eff}}$, shown in Fig. 3; good agreement was found with theoretical calculations [9]. In the slow-light regime, we observed a maximum $\Delta n_g \sim 68$, implying a group velocity (v_g) of 4411 km/s at $P_p \sim 152$ mW. For a signal centered at ω_{as}, the slope of $n(\omega)$ is negative (see Fig. 1), leading to negative values of n_g. In the fast-light regime, a maximum $\Delta n_g \sim -44$ was measured at $P_p \sim 91$ mW, which was lower than that for the slow-light measurement, as the increased absorption at a large P_p makes the measurement difficult. From the measured $\Delta n_g(\omega_{\text{as}})$ we obtain a negative $v_g \sim -6818$ km/s. To the best of our knowledge, such large slow- and fast-light group indices have never been observed using SBS.

To measure the pulse delays, we modulated the probe with a Gaussian pulse. For these experiments we used a pulsed pump to increase the on-chip pump power to ~300 mW. Pump pulses were 1 μs long with a duty cycle of 20% and were synchronized with the probe pulses.

Figures 4(a) and 4(b) show the delay for FWHM pulse widths of ~25 and ~100 ns, respectively, for different values of gain ($G = g_B I_p L_{\text{eff}}$). As the pump power was increased, the gain (absorption) increased, and thus the group index increased (decreased) and the speed of light pulse was reduced (advanced) for pulses centered at ω_s (ω_{as}), resulting in slow and fast light. For a 25 ns long Gaussian pulse, we achieved a delay of ~22 ns at $G \sim 4.9$, while for a 100 ns long Gaussian pulse the maximum delay was ~23 ns at $G \sim 5.3$. From the measured slow-light delay for a 100 ns pulse, we calculated the maximum achieved Δn_g to be ~130, which was approximately twice the group index measured at the Stokes shift as group delay measurements at ~152 mW (see Fig. 3) and is the largest reduction ever achieved in the speed of light pulses using SBS. The total insertion loss (IL) for the 100 and 25 ns pulse delay measurements was ~10.5 and ~12.5 dB, respectively, which includes ~4 dB coupling loss at each facet and a total loss of input and output circulators ~0.8 dB. Using the loss estimate, the effective lengths for the 100 and 25 ns pulses were estimated to be ~5.5 and ~4.7 cm, respectively. We attribute the higher insertion loss for the 25 ns pulse to the

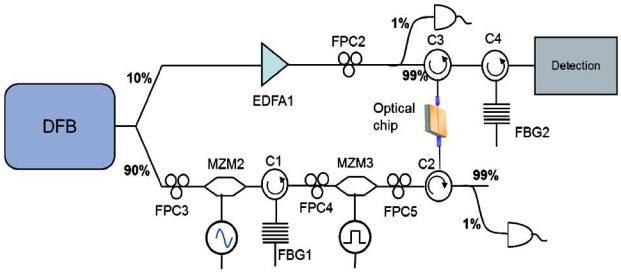

Fig. 2. (Color online) Experimental setup for SBS slow/fast light. DFB, distributed feedback laser; EDFA, erbium-doped fiber amplifier; FPC, fiber polarization controller; FBG, fiber Bragg grating; MZM, Mach–Zehnder modulator; C1–5, circulator.

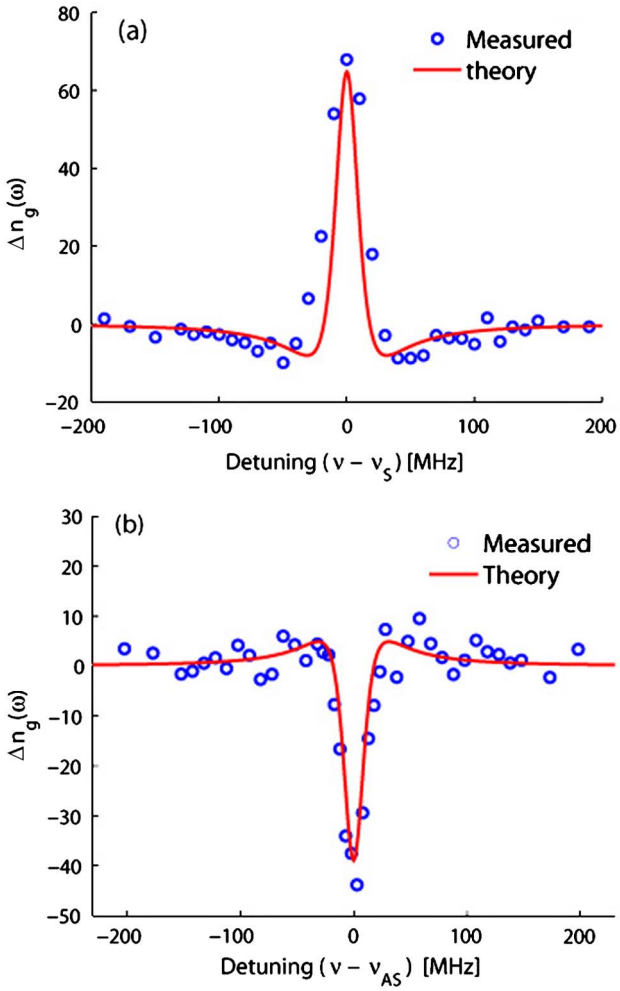

Fig. 3. (Color online) Calculated (solid curves) and measured (circles) group index profile for (a) slow light and (b) fast light. A sinusoidal modulation of 10 MHz for slow light and 3 MHz for fast light was imposed on the probe carrier wave, whose frequency was detuned from the Stokes (anti-Stokes) for slow (fast) light. The coupled CW pump powers of ~152 mW for slow light and ~91 mW for fast light were used.

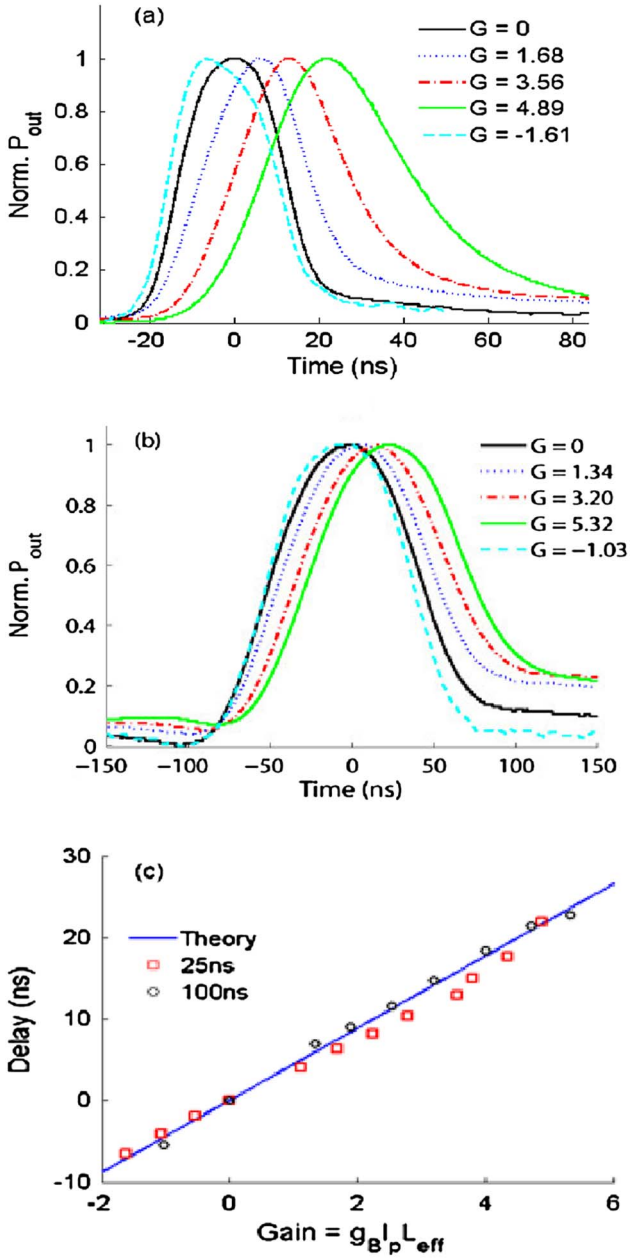

Fig. 4. (Color online) Measured output pulses for different gain values demonstrating SBS induced slow and fast light for (a) a 25 ns Gaussian pulse and (b) a 100 ns Gaussian pulse and (c) measured and theoretical delay, obtained using Eq. (1), versus gain.

alignment of the pump and probe polarizations with the increased loss of the TM mode.

For fast-light pulse delay experiments we only used a CW pump. For a 100 ns pulse, a maximum pulse advance of ~ – 6 ns was obtained at $G \sim -1.03$. The output pulses for the 25 ns probe pulse exhibit significant broadening for large gain values as the different frequency components experienced different delay and gain, resulting in pulse distortion. For the 100 ns probe pulse the output pulses were nearly the same width as the input pulse. The detector response, however, introduced a long tail in the trailing edge of the input and slow/fast pulses. We attribute the origin of this tail to a diffusion current in the detector. Figure 4(c) shows a comparison of our measured delay with the theoretical delay calculated using Eq. (1), showing good agreement between theory and experiments for the 100 ns pulse, while the slow-light delay for a 25 ns pulse was slightly smaller, as would be expected.

In conclusion, we have demonstrated on-chip slow, fast, and negative group velocities using SBS where Δn_g was continuously varied from −44 to +130, resulting in $v_g \sim 2307$ km/s and −6818 km/s.This demonstration opens up on-chip SBS devices for applications where multiple delay lines with tunable delays of ~10 ns are required, e.g., phased array antenna [2]. Furthermore, the large dispersion offers increased sensitivity for ultracompact spectrometers [15].

This work was funded by the Australian Research Council (ARC) through its Discovery grant (DP1096838), Federation fellowship, and Center of Excellence CUDOS, and by the U.S. Department of Defense through AFOSR/AOARD (grant #FA23861114030).

References

1. R. W. Boyd and D. J. Gauthier, Science **326**, 1074 (2009).
2. S. Chin, L. Thevenaz, J. Sancho, S. Sales, J. Capmany, P. Berger, and J. Bourderionnet, Opt. Express **18**, 22599 (2010).
3. Y. Okawachi, M. S. Bigelow, J. E. Sharping, Z. M. Zhu, A. Schweinsberg, D. J. Gauthier, R. W. Boyd, and A. L. Gaeta, Phys. Rev. Lett. **94**, 153902 (2005).
4. R. Pant, M. D. Stenner, M. A. Neifeld, and D. J. Gauthier, Opt. Express **16**, 2764 (2008).
5. Z. Shi, R. Pant, Z. Zhu, M. D. Stenner, M. A. Neifeld, D. J. Gauthier, and R. W. Boyd, Opt. Lett. **32**, 1986 (2007).
6. K. Y. Song and K. Hotate, Opt. Lett. **32**, 217 (2007).
7. L. Thevenaz, Nat. Photon. **2**, 474 (2008).
8. Y. H. Zhu, M. Lee, M. A. Neifeld, and D. J. Gauthier, Opt. Express **19**, 687 (2011).
9. Z. M. Zhu and D. J. Gauthier, J. Opt. Soc. Am. B **22**, 2378 (2005).
10. K. S. Abedin, G. W. Lu, and T. Miyazaki, Electron. Lett. **44**, 16 (2008).
11. K. Y. Song, K. S. Abedin, K. Hotate, M. G. Herraez, and L. Thevenaz, Opt. Express **14**, 5860 (2006).
12. E. Cabrera-Granado, O. G. Calderon, S. Melle, and D. J. Gauthier, Opt. Express **16**, 16032 (2008).
13. B. J. Eggleton, B. Luther-Davies, and K. Richardson, Nat. Photon. **5**, 141 (2011).
14. R. Pant, C. G. Poulton, D.-Y. Choi, H. Mcfarlane, S. Hile, E. Li, L. Thevenaz, B. Luther-Davies, S. J. Madden, and B. J. Eggleton, Opt. Express **19**, 8285 (2011).
15. S. Sternklar, E. Sarid, M. Wart, and E. Garnot, J. Opt. **12** (2010).

Photonic chip based tunable and reconfigurable narrowband microwave photonic filter using stimulated Brillouin scattering

Adam Byrnes,[1] Ravi Pant,[1] Enbang Li,[1] Duk-Yong Choi,[2] Christopher G. Poulton,[3] Shanhui Fan,[1,4] Steve Madden,[2] Barry Luther-Davies,[2] and Benjamin J. Eggleton[1,*]

[1]*Centre for Ultrahigh bandwidth Devices for Optical Systems (CUDOS), Institute of Photonics and Optical Science (IPOS), School of Physics, The University of Sydney, NSW 2006, Australia*
[2]*CUDOS, Laser Physics Centre, Australian National University, Canberra, ACT 0200, Australia*
[3]*CUDOS, University of Technology Sydney, Sydney, NSW 2007, Australia*
[4]*Department of Electrical Engineering, Stanford University, Stanford, California 94305, USA*
** egg@physics.usyd.edu.au*

Abstract: We report the first demonstration of a photonic chip based dynamically reconfigurable, widely tunable, narrow pass-band, high Q microwave photonic filter (MPF). We exploit stimulated Brillouin scattering (SBS) in a 6.5 cm long chalcogenide (As_2S_3) photonic chip to demonstrate a MPF that exhibited a high quality factor of ~520 and narrow bandwidth and was dynamically reconfigurable and widely tunable. It maintained a stable 3 dB bandwidth of 23 ± 2MHz and amplitude of 20 ± 2 dB over a large frequency tuning range of 2-12 GHz. By tailoring the pump spectrum, we reconfigured the 3 dB bandwidth of the MPF from ~20 MHz to ~40 MHz and tuned the shape factor from 3.5 to 2 resulting in a nearly flat-topped filter profile. This demonstration represents a significant advance in integrated microwave photonics with potential applications in on-chip microwave signal processing for RADAR and analogue communications.

OCIS codes: (190.2640) Stimulated scattering, modulation; (190.4390) Nonlinear optics, integrated optics; (060.5625) Radio frequency photonics.

References and links

1. J. Capmany, B. Ortega, and D. Pastor, "A tutorial on microwave photonic filters," J. Lightwave Technol. **24**(1), 201–229 (2006).
2. D. B. Hunter and R. A. Minasian, "Tunable microwave fiber-optic bandpass filters," IEEE Photon. Technol. Lett. **11**(7), 874–876 (1999).
3. Y. M. Chang and J. H. Lee, "High-Q tunable, photonic microwave single passband filter based on stimulated Brillouin scattering and fiber Bragg grating filtering," Opt. Commun. **281**(20), 5146–5150 (2008).
4. X. Yi and R. A. Minasian, "Microwave photonic filter with single bandpass response," Electron. Lett. **45**(7), 362–U31 (2009).
5. W. Li, M. Li, and J. Yao, "A narrow-passband and frequency-tunable microwave photonic filter based on phase-modulation to intensity-modulation conversion using a phase-shifted fiber Bragg grating," IEEE Trans. Microw. Theory Tech. **60**(5), 1287–1296 (2012).
6. M. Bolea, J. Mora, B. Ortega, and J. Capmany, "Highly chirped single-bandpass microwave photonic filter with reconfiguration capabilities," Opt. Express **19**(5), 4566–4576 (2011).
7. J. Mora, B. Ortega, A. Diez, J. L. Cruz, M. V. Andres, J. Capmany, and D. Pastor, "Photonic microwave tunable single-bandpass filter based on a Mach-Zehnder interferometer," J. Lightwave Technol. **24**(7), 2500–2509 (2006).
8. K. Zhu, H. Ou, H. Fu, E. Remb, and S. He, "A simple and tunable single-bandpass microwave photonic filter of adjustable shape," IEEE Photon. Technol. Lett. **20**(23), 1917–1919 (2008).
9. V. R. Supradeepa, C. M. Long, R. Wu, F. Ferdous, E. Hamidi, D. E. Leaird, and A. M. Weiner, "Comb-based radiofrequency photonic filters with rapid tunability and high selectivity," Nat. Photonics **6**(3), 186–194 (2012).
10. A. J. Torregrosa, H. Maestre, A. L. Recas, J. A. Pereda, J. Capmany, and C. R. Fernandez-Pousa, "Tunability of the multiple-bandpass response of cascaded single-source and continuous-sample microwave photonic filters," Opt. Commun. **283**(7), 1320–1325 (2010).

#170558 - $15.00 USD Received 13 Jun 2012; revised 23 Jul 2012; accepted 30 Jul 2012; published 1 Aug 2012

11. X. Xue, X. Zheng, H. Zhang, and B. Zhou, "Single-bandpass microwave photonic filter with wide tuning range and no baseband response," IEEE Photonics Conference 143–144 (2011).
12. J. Mora, J. Capmany, and L. R. Chen, "Tunable and reconfigurable single bandpass photonic microwave filter using a high-birefringence Sagnac loop and DVMM channel selector," IEEE Leos Annual Meeting **1-2**, 192–193 (2007).
13. B. Vidal, M. A. Piqueras, and J. Martí, "Tunable and reconfigurable photonic microwave filter based on stimulated Brillouin scattering," Opt. Lett. **32**(1), 23–25 (2007).
14. W. W. Zhang and R. A. Minasian, "Widely tunable single-passband microwave photonic filter based on stimulated Brillouin scattering," IEEE Photon. Technol. Lett. **23**(23), 1775–1777 (2011).
15. J. Sancho, Sanghoon Chin, M. Sagues, A. Loayssa, J. Lloret, I. Gasulla, S. Sales, L. Thévenaz, and J. Capmany, "Dynamic microwave photonic filter using separate carrier tuning based on stimulated Brillouin scattering in fibers," IEEE Photon. Technol. Lett. **22**(23), 1753–1755 (2010).
16. B. Vidal, T. Mengual, and J. Marti, "Photonic microwave filter with single bandpass response based on Brillouin processing and SSB-SC," International Topical Meeting on Microwave Photonics 92–95 (2009).
17. A. Loayssa, J. Capmany, M. Sagues, and J. Mora, "Demonstration of incoherent microwave photonic filters with all-optical complex coefficients," IEEE Photon. Technol. Lett. **18**(16), 1744–1746 (2006).
18. B. J. Eggleton, B. Luther-Davies, and K. Richardson, "Chalcogenide Photonics," Nat. Photonics **5**, 141–148 (2011).
19. B. J. Eggleton, T. D. Vo, R. Pant, J. Schr, M. D. Pelusi, D. Yong Choi, S. J. Madden, and B. Luther-Davies, "Photonic chip based ultrafast optical processing based on high nonlinearity dispersion engineered chalcogenide waveguids," Laser Photon. Rev. **6**(1), 97–114 (2012).
20. W. J. Chin, D. H. Kim, J. H. Song, and S. S. Lee, "Integrated photonic microwave bandpass filter incorporating a polymeric microring resonator," JJAP Part 1-Regular Papers Brief Communications & Review Papers **45**(4A), 2576–2579 (2006).
21. F. Coppinger, C. K. Madsen, and B. Jalali, "Photonic microwave filtering using coherently coupled integrated ring resonators," Microw. Opt. Technol. Lett. **21**(2), 90–93 (1999).
22. E. J. Norberg, R. S. Guzzon, J. S. Parker, L. A. Johansson, and L. A. Coldren, "Programmable photonic microwave filters monolithically integrated in InP-InGaAsP," J. Lightwave Technol. **29**(11), 1611–1619 (2011).
23. R. Pant, A. Byrnes, C. G. Poulton, E. Li, D.-Y. Choi, S. Madden, B. Luther-Davies, and B. J. Eggleton, "Photonic-chip-based tunable slow and fast light via stimulated Brillouin scattering," Opt. Lett. **37**(5), 969–971 (2012).
24. R. Pant, C. G. Poulton, D.-Y. Choi, H. Mcfarlane, S. Hile, E. Li, L. Thevenaz, B. Luther-Davies, S. J. Madden, and B. J. Eggleton, "On-chip stimulated Brillouin scattering," Opt. Express **19**(9), 8285–8290 (2011).
25. R. Pant, M. D. Stenner, M. A. Neifeld, Z. M. Shi, R. W. Boyd, and D. J. Gauthier, "Maximizing the opening of eye diagrams for slow-light systems," Appl. Opt. **46**(26), 6513–6519 (2007).

1. Introduction

Microwave filters form a critical part of microwave signal processing with applications in RADAR, radio over fiber (RoF), and mobile communications [1]. However, microwave filters implemented in the electrical domain suffer from electromagnetic interference (EMI), are difficult to tune and difficult to reconfigure in terms of the filter shape and its bandwidth [1]. Microwave *photonic* filters (MPFs), on the other hand, can provide a wide tuning range, are naturally immune to EMI, and some schemes exhibit the ability to be reconfigured [1]. In recent years, a number of MPF designs exhibiting either a periodic transfer function or a single pass-band have been demonstrated in optical fiber. These MPFs have been based on tapped delay lines and single pass-band architectures, realized using technologies such as Fiber Bragg Gratings (FBGs) [2–5]; Mach-Zehnder interferometers (MZIs) [6–8]; dispersion based tap delay [9, 10]; semiconductor optical amplifiers (SOAs) [11]; Sagnac loops [12]; or stimulated Brillouin scattering (SBS) [13–17].

When the MPF has a periodic transfer function, the tuning range is obviously limited by the free spectral range (FSR) and this also restricts the amount by which the bandwidth can be reconfigured. MPFs with a single pass-band are, therefore, better suited for applications where large tuning and large dynamic bandwidth are required [1]. Recently widely tunable single pass-band MPFs with high Q have been demonstrated by exploiting the narrow gain spectrum of SBS [13, 14, 16]. However, these impressive results were achieved in an optical fiber ~10-20 km long [13, 14, 16, 17] which makes them incompatible with all-optical integration [18, 19]. Quite impressive results have also been reported using chip-based photonic microwave signal processors, however, current MPF bandwidths have been limited to > 1 GHz and a Q factor of ~10 [20–22].

#170558 - $15.00 USD Received 13 Jun 2012; revised 23 Jul 2012; accepted 30 Jul 2012; published 1 Aug 2012

In this paper we report the first demonstration of an on-chip tunable, narrowband microwave photonic filter with a high Q. We also demonstrate that the shape and bandwidth of such a filter can be easily reconfigured. In this work we exploited the large SBS gain coefficient (g_B ~0.74 x 10^{-9} m/W) [23, 24] and small effective mode area (~2.3 μm^2) of an As_2S_3 rib waveguide to achieve large SBS gain in a 6.5 cm long rib waveguide at moderate pump power (~300mW). Our device provided a narrow 3dB bandwidth f_{3dB} ~23 ± 2MHz with stable amplitude ~20 ± 2 dB over a wide frequency range (2-12 GHz) resulting in a Q ~520: 52 times the Q values previously reported for on-chip MPFs [21]. The shape factor (S) of the MPF, which is defined as the ratio of −20 dB to −3 dB bandwidth, was also tuned from 3.5 to 2 by tailoring the pump profile [13, 25]. This demonstration represents a significant advance in the field of integrated microwave photonics.

2. Principle of operation

In this section we present the principle of operation of our microwave photonic filter. This principle was first demonstrated in [14] for the case of a long optical fiber. Here we review the basic operating principle, which is illustrated in Fig. 1, and also discuss some specific aspects that are unique to our device based on an As_2S_3 photonic chip.

In Fig. 1, a microwave signal A(Ω) is first encoded into an optical carrier (ω_o) using phase modulation. The phase encoding results in equal amplitude upper and lower sidebands that are out of phase by π. The beat signals between these out-of-phase sidebands and the carrier interfere destructively and, hence, no filtered signal appears in the microwave spectrum. However, when one of the side bands is amplified using SBS, the beat signals have different amplitudes and no longer cancel, resulting in the generation of a filtered signal in the microwave domain that has the spectrum and bandwidth of the SBS gain profile (see Fig. 1).

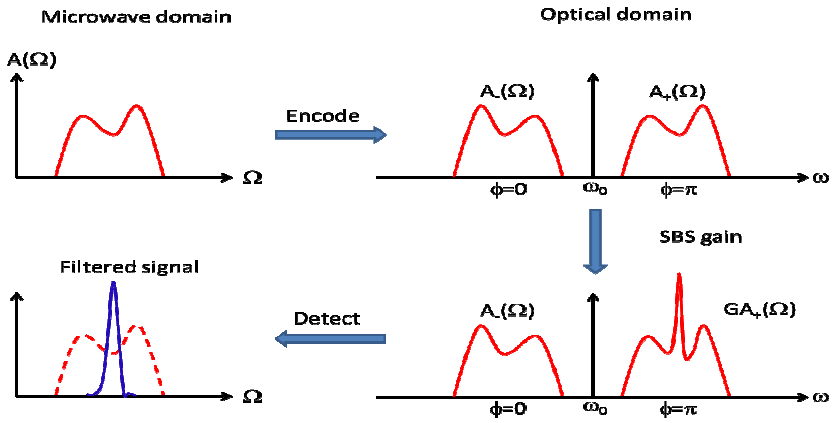

Fig. 1. Principle of stimulated Brillouin scattering based microwave photonic filter

The key to our photonic chip based microwave photonic filter (PCMPF) is the strong SBS cross-section (g_B) and small effective optical mode area (A_{eff}) of our chalcogenide (As_2S_3) waveguide [23, 24]. For SBS, the gain exponent $G = g_B P_p L_{eff}/A_{eff}$ depends on both g_B, and the pump intensity $I_p = P_P/A_{eff}$, where P_p is the pump power, and effective length L_{eff}. To achieve large SBS gain in a short device at moderate pump powers, therefore, requires a material with large g_B and a device with small A_{eff}. The gain coefficient g_B is enhanced using high refractive index materials, because g_B scales with n^8. Further enhancement can be achieved by ensuring that the photons and phonons are both guided within the same structure. An As_2S_3 chalcogenide glass waveguide satisfies these conditions [18] having a large refractive index n = 2.43 at 1550nm, which results in large g_B and also allows tight confinement of both the optical and acoustic modes in a rib waveguide structure. For our chalcogenide chip g_B ~0.74 x 10^{-9} m/W (~70 x silica) and A_{eff} = 2.3 μm^2, which results in large G at small pump powers.

#170558 - $15.00 USD Received 13 Jun 2012; revised 23 Jul 2012; accepted 30 Jul 2012; published 1 Aug 2012

3. Theory

Next we present a generalized theory of a MPF exploiting SBS and phase modulation of an optical carrier. The theory considers filtering of an arbitrary microwave signal A(Ω) instead of a sinusoidal signal and analyses the effect of any unwanted signals that may arise due to beating of the phase modulated signal with a co-propagating parasitic pump, introduced by the reflection at the lensed fiber-chip interface.

First we consider the ideal case of Fig. 1 where a microwave signal A(Ω) is phase encoded onto an optical carrier (ω_o) and filtered using SBS. After encoding, the resulting optical signal is given as:

$$E(t) = e^{j\omega_0 t} e^{j\phi(t)} = e^{j\omega_0 t}\left[1 + \int_{-\infty}^{\infty} A_{-}(\Omega) e^{-j\Omega t} d\Omega + \int_{-\infty}^{\infty} A_{+}(\Omega) e^{j\Omega t} d\Omega\right]. \quad (1)$$

Using the fact that for a phase modulated signal the intensity $I(t) = |E(t)|^2$ = constant, the contribution from non-DC terms must be zero. Assuming small-signal modulation and considering only the first order non-DC terms in I(t), we obtain:

$$\int_{-\infty}^{\infty}\left[A_{-}^{*}(\Omega) + A_{+}(\Omega)\right] e^{j\Omega t} d\Omega = 0, \quad (2)$$

which implies that for a phase modulated signal $A^*_{-}(\Omega) = -A_{+}(\Omega)$. This condition arises because no signal should appear on the radio frequency spectrum analyzer (RFSA) for a pure phase modulated signal.

When the SBS gain is applied to one of the phase modulated side bands (e.g. the upper sideband), the signal on the RFSA (assuming small-signal modulation) arises from the following non-DC terms:

$$I(t) \approx \int_{-\infty}^{\infty}\left[A_{-}^{*}(\Omega) + G(\Omega) A_{+}(\Omega)\right] e^{j\Omega t} d\Omega. \quad (3)$$

Using the fact that $A^*_{-}(\Omega) = -A_{+}(\Omega)$ in Eq. (3), the detected signal is given by:

$$I(t) \approx \int_{-\infty}^{\infty}\left(G(\Omega) - 1\right) A_{+}(\Omega) e^{j\Omega t} d\Omega. \quad (4)$$

From Eq. (4), it is evident that the output in the microwave domain has a spectrum $[G(\Omega)-1]A_{+}(\Omega)$ and thus, with respect to the input microwave signal A(Ω), the output microwave signal is filtered by the SBS gain response G(Ω)-1.The result in Eq. (4) shows that in the ideal case of Fig. 1, under the small-signal modulation approximation i.e. higher-order non-DC terms are neglected, the SBS process can be used to filter a microwave signal.

In our specific implementation that will be discussed in more detail below, due to the reflections at the ends of the chip, the injected counter-propagating pump generates a parasitic pump co-propagating with the phase modulated signal. Below we analyze the degradation of the filter response due to such a parasitic effect.

In order to analyze this non-ideal case, shown in Fig. 2, we rewrite Eq. (1) in the presence of a co-propagating backscattered pump with gain on the upper phase modulated sideband as:

$$E(t) = e^{j\omega_0 t}\left[1 + \int_{-\infty}^{\infty} A_{-}(\Omega) e^{-j\Omega t} d\Omega + \int_{-\infty}^{\infty} G(\Omega) A_{+}(\Omega) e^{j\Omega t} d\Omega + A_p e^{j(\omega_p - \omega_0)t}\right]. \quad (5)$$

#170558 - $15.00 USD Received 13 Jun 2012; revised 23 Jul 2012; accepted 30 Jul 2012; published 1 Aug 2012

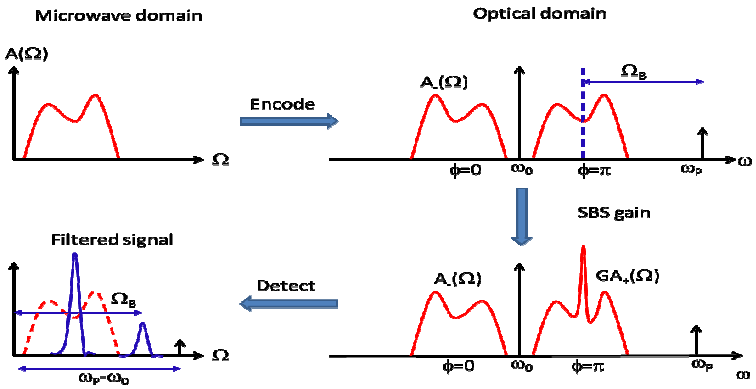

Fig. 2. Schematic of stimulated Brillouin scattering based microwave photonic filter with residual co-propagating pump which arises due to reflection at the lensed fiber and chip interface.

Once again assuming small-signal modulation and considering only the first-order non-DC terms in I(t), we obtain:

$$I(t) \approx \underbrace{\int_{-\infty}^{\infty} \left(G(\Omega)-1\right) A_{+}(\Omega) e^{j\Omega t} d\Omega}_{\text{Filtered Signal}} + \underbrace{\left[\begin{array}{c} A_p e^{j(\omega_p-\omega_0)t} + \int_{-\infty}^{\infty} A_p A_{-}^{*}(\Omega) e^{j(\omega_p-\omega_0+\Omega)t} d\Omega + \\ \int_{-\infty}^{\infty} A_p G^{*}(\Omega) A_{+}^{*}(\Omega) e^{j(\omega_p-\omega_0-\Omega)t} d\Omega \end{array} \right]}_{\text{Unwanted Signals}}. \quad (6)$$

The first term in Eq. (6) represents the filter operation as derived in Eq. (4). The remaining terms in Eq. (6) contribute to the degradation of the filter response by generating undesired signals. The second term arises from the beating between the carrier and residual pump and gives rise to a signal at ω_p - ω_0; the third term arises from the beating between the residual pump and unamplified sideband; and the final term results from beating between amplified sideband and the residual pump, which results in a microwave signal at the Brillouin shift Ω_B. In order to reduce these unwanted signals, we removed the parasitic pump signal at the output using a Bragg grating, however, there is still some residual pump which generates a small amount of unwanted beat signals. Furthermore, a small signal is generated from beating between the amplified and unamplified PM sideband. These unwanted terms, however, arise from practical constraints such as stray or scattered light from the pump, which can be eliminated by improving coupling into the rib waveguide using, for example, on-chip tapers.

4. Experiment

4.1 Set up

Figure 3 shows the experimental set up used to realize a PCMPF. Continuous wave (CW) light from a distributed feedback (DFB) laser was passed through an isolator and then split into two parts using a 99/1 coupler. The 1% port became the "pump arm" and was amplified using a 2W C-band EDFA (EDFA1) and passed through a polarization controller (PC1) before being launched into the chip via a circulator (C1) and a lensed fiber. The 99% port was used to generate a carrier suppressed intensity modulated signal using an intensity modulator (IM), which split the light into upper and lower sidebands. One of the IM sidebands was removed using a fiber Bragg grating (FBG1) before it entered a 90/10% coupler. The 90% port acted as the optical carrier on which the RF signal was encoded using a phase modulator (PM). The PM signal was then coupled into the chip via C2 and a lensed fiber. The

#170558 - $15.00 USD Received 13 Jun 2012; revised 23 Jul 2012; accepted 30 Jul 2012; published 1 Aug 2012

polarization of light going into the phase modulator and the chip was controlled using polarization controllers PC3 and PC5 respectively. The 10% arm was amplified using a low-noise EDFA (EDFA2), and passed through a polarization controller (PC4). The output of the chip was collected through circulator C1 and passed through FBG2, where the back-reflected pump due to reflections at the end faces of the chip was removed. The signal after pump removal was then coupled with the amplified carrier wave using a 50/50 coupler, one arm of which lead to an OSA and the other to a high-speed photo detector connected to a RFSA. The power of the re-injected amplified optical carrier was kept fixed throughout the experiment. The rib waveguide used in the experiments was 6.5 cm long with a cross-section of 4 µm x 850 nm with anti-reflection coatings applied to the end facets. The Brillouin shift of the chalcogenide (As_2S_3) chip is ~7.7 GHz.

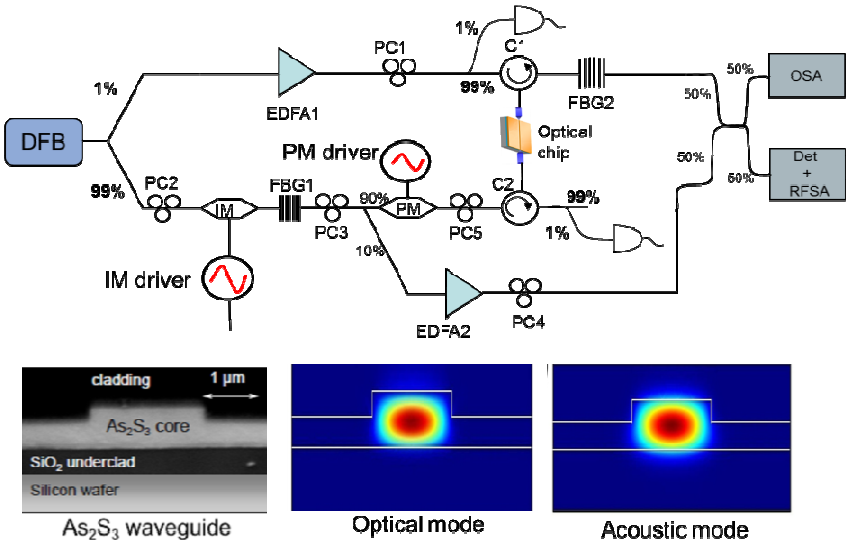

Fig. 3. Experimental setup to realize PCMPF using SBS along with the optical microscope image of a typical rib waveguide and optical and acoustic modes in the rib structure showing strong optical-acoustic confinement. PC: polarization controller, FBG: fiber Bragg grating, IM: intensity modulator, PM: phase modulator C: circulator, EDFA: erbium doped fiber amplifier, OSA: optical spectrum analyser, Det: photodetector and RFSA: radio frequency spectrum analyser.

4.2 General operation

In the experiment to demonstrate the PCMPF, the Brillouin pump frequency was kept fixed at the laser frequency (ω_L) while the frequency of the carrier, on which the RF signal (ω_{RF}) was phase encoded, was tuned using an intensity modulator (IM). The intensity modulator was biased to suppress the laser frequency as shown in Figs. 4(a) and 4(c). In the case when the RF frequency ω_{RF} was smaller than the frequency (ω_M) of the IM, the lower IM side band was used as the carrier while the upper IM sideband was removed using a tunable fiber Bragg grating (FBG1) as shown in Fig. 4(a). In this case, the upper phase modulated sideband experienced gain (see Fig. 4(b)). The parasitic pump, which originated from reflections at the interface of lens fiber and chip was removed using FBG2 (see Fig. 4(b)). The MPF center frequency (ω_{RF}) could be tuned in the range from 0 to $\omega^{max}_M - \Omega_B$, where ω^{max}_M is the maximum frequency determined by the IM and its driver. In our experiment the maximum frequency of the IM driver was ω^{max}_M = 15 GHz and therefore the MPF tuning range for this case i.e. when $\omega_M > \omega_{RF}$ was restricted from 0 to $\omega^{max}_M - \Omega_B$ ~7.2 GHz. In order to increase the tuning range beyond $\omega^{max}_M - \Omega_B$, we operated in a region where $\omega_M < \omega_{RF}$. Note that a single-sideband (SSB) IM and a signal generator with larger ω^{max}_M would provide much larger

#170558 - $15.00 USD Received 13 Jun 2012; revised 23 Jul 2012; accepted 30 Jul 2012; published 1 Aug 2012

tuning range without going into the $\omega_M < \omega_{RF}$ operating regime. This would also simplify the device operation by avoiding the need for FBG1.

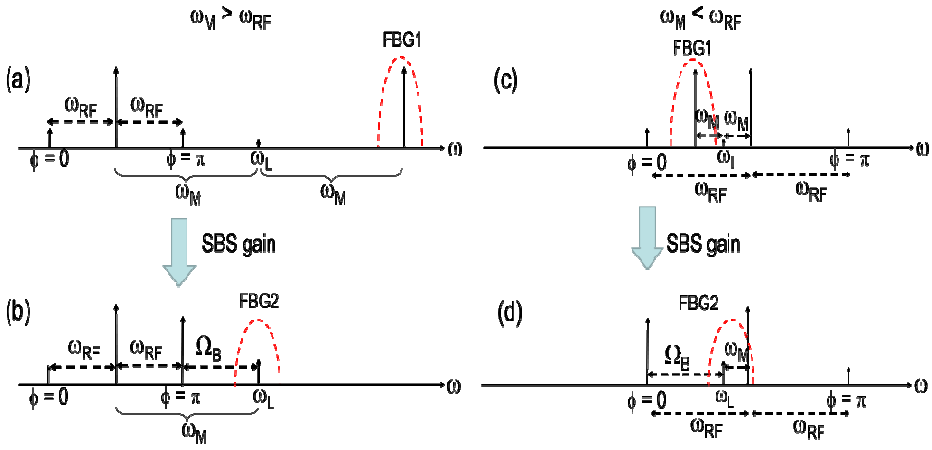

Fig. 4. Principle of general MPF operation when IM frequency greater than RF frequency $\omega_M > \omega_{RF}$ (a, b) and for IM frequency smaller than RF frequency $\omega_{RF} > \omega_M$ (c, d). For $\omega_M > \omega_{RF}$, lower IM sideband is used as a carrier for phase modulation and the upper phase modulated sideband experiences SBS gain. For $\omega_{RF} > \omega_M$, upper IM sideband acts as the carrier for phase modulation and lower phase modulated sideband experiences SBS gain. For $\omega_M > \omega_{RF}$, the IM carrier is blocked by FBG2, which was used to remove the parasitic pump.

When $\omega_M < \omega_{RF}$, the upper IM sideband acted as the optical carrier on which the RF signal was phase modulated while the lower IM sideband was removed using a FBG (see Fig. 4(c)). In this case, the lower PM sideband experienced gain (see Fig. 4(d)) and the MPF center frequency could be tuned from $\omega^{min}_M + \Omega_B$ to $\omega^{max}_M + \Omega_B$, where ω^{min}_M is the minimum frequency of the signal generator driving the IM. In our experiment, the maximum MPF tuning frequency was restricted to 12 GHz because both the phase modulator and its driver have a maximum range of 12 GHz. The lowest MPF center frequency in this operating regime ($\omega_M < \omega_{RF}$) was limited by the lowest frequency (ω^{min}_M) of the IM driver. The ω^{min}_M of 2 GHz restricted the lowest MPF frequency for this operating regime to ~10 GHz. Thus, the PCMPF could not be operated at 8 and 9 GHz in these experiments, however, this constraint is not a fundamental limitation of the system.

For both the operation regimes i.e. $\omega_M < \omega_{RF}$ and $\omega_M > \omega_{RF}$, the optical carrier wave was reintroduced after removing the residual back-reflected pump using FBG2. The reintroduced carrier makes up for the reduced carrier power after propagation through the chip where ~12 dB insertion loss was experienced by the phase modulated signal. The coupling to the chip was performed using lens-tip fibers with a spot size of 2.5 μm, which resulted in ~4dB coupling loss at each facet. For $\omega_M < \omega_{RF}$, the IM carrier was suppressed by the FBG2 (see Fig. 4(d)). A fixed carrier power was reintroduced for both the operating regimes before detection.

4.3 Filter tuning

Figure 5 shows the RFSA trace when a phase modulated (PM) signal centered at $\omega_{RF} = 7$ GHz counter-propagated with a pump such that the upper PM sideband was downshifted from the pump by Ω_B. In this condition the gain experienced by the upper PM sideband resulted in large amplitude mismatch between the two out-of-phase sidebands creating a large signal (~20 dB) on the RFSA at $\omega_{RF} = 7$ GHz. As predicted in the theory section, a small unwanted signal (~1.3dB) appeared at Ω_B (see inset Fig. 5), due to beating of the residual backscattered pump with the amplified PM sideband. Another small signal (~2.2 dB) appeared at $2\omega_{RF} = 14$ GHz, due to beating between the amplified and unamplified sidebands. The extinction measured in

#170558 - $15.00 USD Received 13 Jun 2012; revised 23 Jul 2012; accepted 30 Jul 2012; published 1 Aug 2012

comparison to the noise level is ~20 ± 2 dB. However, the unwanted beat signals, predicted by Eq. (6) and shown in the inset of Fig. 5 reduced the sideband suppression by ~3dB.

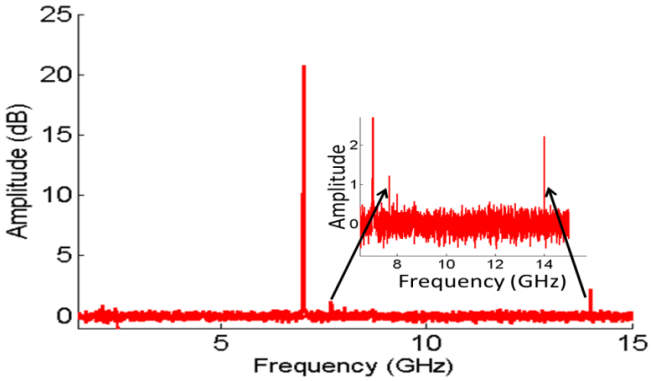

Fig. 5. RF trace for filtering of a phase modulated RF signal centered at ω_{RF} = 7 GHz using PCMPF showing a large signal ~20 dB on the RFSA at the RF frequency ω_{RF} = 7GHz and other small unwanted signals arising from the beating of residual co-propagating pump with amplified signal (Ω_B) and a signal arising from beating between the amplified and unamplified PM sideband at $2\omega_{RF}$ = 14 GHz (see inset).

With the pump off, a small signal (~4dB) appeared at ω_{RF} = 7GHz on the RFSA. We attributed this to imbalance between the power in the upper and lower PM sidebands due to asymmetry in the modulator and the presence of the grating (FBG2), which affected the sidebands differently. This resulted in incomplete cancellation of the out-of phase beat signals.

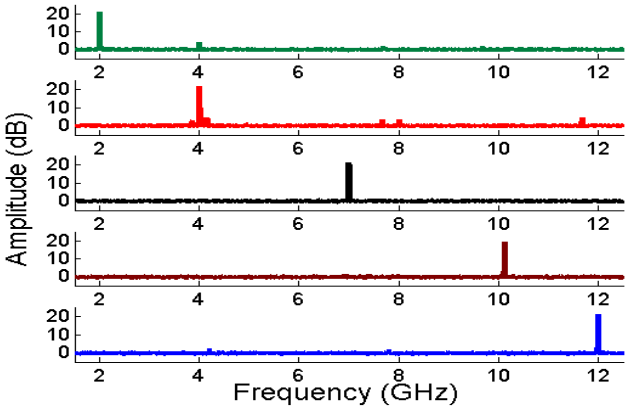

Fig. 6. Tuning response of the MPF centre frequency over the range 2-12 GHz demonstrating wide tuning range.

To tune the MPF center frequency, we tuned both the IM frequency and the PM driver frequency so that one PM sideband was always at the Brillouin shift from the pump. Figure 6 shows that the PCMPF could be tuned over a wide range (2-12GHz). A constant SBS gain of ~20dB was used to obtain Fig. 6. The amplitude and bandwidth fluctuations in the MPF response over the tuning range are shown in Fig. 7 demonstrating good amplitude (~20 ± 2 dB) and bandwidth (f_{3dB} ~23 ± 2 MHz) stability. The inset in Fig. 7 shows the MPF profiles centered at RF frequencies of 4 GHz and 11 GHz, obtained by scanning the PM driver frequency over 1 GHz. The maximum Q-factor, defined as the MPF center frequency divided by the f_{3dB}, was calculated to be ~520 for a RF center frequency of 12 GHz.

#170558 - $15.00 USD Received 13 Jun 2012; revised 23 Jul 2012; accepted 30 Jul 2012; published 1 Aug 2012

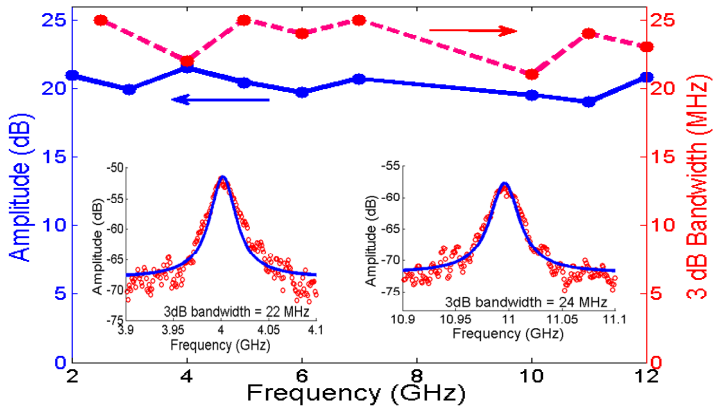

Fig. 7. Amplitude and 3dB bandwidth of PCMPF for different centre RF frequencies demonstrating good amplitude (~20 ± 2 dB) and bandwidth (23 ± 2 MHz) stability. Inset: MPF profiles taken at centre frequencies of 4 and 11 GHz.

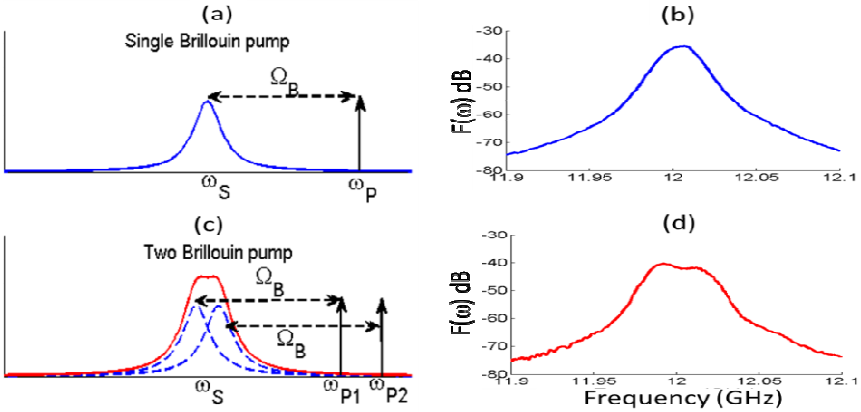

Fig. 8. Theoretical filter response for (a) single and (c) two pumps demonstrating MPF profile reshaping (flat top) with improved 3dB bandwidth. Measured MPF profiles for (b) single pump f_{3dB} ~20 MHz and (d) dual pump f_{3dB} ~40 MHz with shape factor improved from S = 3.5 (single pump) to S = 2 (dual pump). The reshaping results in flat topped filter profile.

To reconfigure the MPF 3dB bandwidth and shape factor, S, we tailored the pump profile [13, 25]. Figures 8(a) and 8(c) show that when we changed the pump spectrum from a single to dual-pump configuration the overall MPF profile (solid Fig. 8(c)), which results from the overlap of two individual gain profiles (dashed Fig. 8(c)), has a flat top and larger f_{3B}. Figures 8(b) and 8(d) show the measured PCMPF profiles for single and dual pumps (separated by 18 MHz), respectively. Using two pumps, a nearly flat-topped MPF profile was achieved with f_{3dB} increased from ~20 MHz to ~40 MHz, which in turn improved S from ~3.5 for a single pump to ~2 for the dual pump.

5. Conclusion

In conclusion, we have presented the first demonstration of a photonic chip based tunable, high Q, narrowband MPF with shape and f_{3dB} reconfiguration. A PCMPF with a stable 3dB bandwidth (~23 ± 2 MHz) and amplitude response (~20 ± 2 dB) over the tuning range of 2-12 GHz was demonstrated. The filter response was reconfigured by tailoring the pump profile, resulting in shape factor enhancement from 3.5 to 2 and f_{3dB} improvement from ~20 MHz to ~40 MHz. The sideband suppression was reduced due to unwanted signals arising from pump reflections. Improved coupling to the chip using, for example, inverse tapers would have

#170558 - $15.00 USD Received 13 Jun 2012; revised 23 Jul 2012; accepted 30 Jul 2012; published 1 Aug 2012

reduced facet reflections and increased the extinction ratio and sideband suppression substantially allowing a simpler experimental set-up by eliminating the need for FBG2. Further, use of a single-sideband intensity modulator with larger modulation frequency would increase the MPF tuning range and further simplify the experiment. This demonstration represents a significant advance in the field of integrated microwave photonics and enables the realization of potential applications in microwave signal processing for radar and analog communications.

Acknowledgments

This work was funded by the Australian Research Council (ARC) through its Discovery grant (DP1096838), Federation fellowship (FF0776056), and Center of Excellence CUDOS (Grant # CE110001018), and by the U.S. Department of Defense through AFOSR/AOARD (grant #FA23861114030).

#170558 - $15.00 USD Received 13 Jun 2012; revised 23 Jul 2012; accepted 30 Jul 2012; published 1 Aug 2012